ORIGINAL ARTICLE

Green synthesis and characterization of Tb-Fe-O-Cu ceramic nanocomposite and its application in simultaneous electrochemical sensing of zinc, cadmium and lead

Hadi Mahmoudi-Moghaddam [a], Mahnaz Amiri [b],**, Hamid Akbari Javar [c], Qahtan A. Yousif [d], Masoud Salavati-Niasari [e],*

[a] Environmental Health Engineering Research Center, Kerman University of Medical Sciences, Kerman, Iran
[b] Neuroscience Research Center, Institute of Neuropharmacology, Kerman University of Medical Science, Kerman, Iran
[c] Pharmaceutics Department, Faculty of Pharmacy, Tehran University of Medical Sciences, Tehran, Iran
[d] Department of Materials, College of Engineering, University of Al-Qadisiyah, Diwaniyah, Iraq
[e] Institute of Nano Science and Nano Technology, University of Kashan, P.O. Box 87317-51167, Kashan, Iran

Abstract In this work, a green technique for preparing $TbFeO_3/CuO$ was reported by employing Crataegus and *Lantana Camara* leaves as fuel and alkalizing agents, respectively. The new sensor based on the perovskite-type nanocomposite was employed as a sensitive and selective platform to detect Pb(II), Zn(II) and Cd(II) simultaneously. $TbFeO_3/CuO/Carbon$ paste electrode (CPE) exhibited a large specific surface area and great electrical conductivity, which enhanced electron transport in the electrochemical process considerably. Moreover, square wave anodic stripping voltammetry (SWASV) was used for the investigation of some factors influencing the sensor sensitivity like pH, modifier concentration, as well as accumulation time and potential. Therefore, the low detection limit (LOD) and a wide linear range were obtained at optimum conditions. In this study, a linear range between 0.9 and 110 µg/L for three ions and LOD of 0.48, 0.29 and 0.12 for zinc, cadmium and lead were achieved, respectively. Moreover, $TbFeO_3/CuO/CPE$ was

* Corresponding author.
** Corresponding author.
E-mail addresses: ma.amiri@kmu.ac.ir (M. Amiri), salavati@kashanu.ac.ir (M. Salavati-Niasari).
Peer review under responsibility of King Saud University.

Production and hosting by Elsevier

employed to detect zinc, cadmium and lead ions simultaneously in the real samples so that the results have shown consistency with a standard inductively coupled plasma (ICP).

1. Introduction

Previous studies have considered heavy metals (HMs) to be strongly toxic and non-biodegradable with abundant distribution, which causes major threats to the biosphere. Excessive HM leads to oxidative stress (OS), impaired anti-oxidant metabolism, and enzyme inhibition (Paithankar et al., 2021). Furthermore, they result in fatal impacts in living organisms through free-radical production and mutations in DNA, lipid peroxidation and a decrease in the protein sulfhydryl (Azeh Engwa et al., 2019; Vardhan et al., 2019). In this regard, Pb (II), which introduces into the environment through agricultural or industrial wastewater causes numerous severe impacts like cancer, coma and kidney disease (Huang et al., 2007). Cd (II) is utilized in pigment and battery industries but higher doses of cadmium ion lead to kidney disease and higher blood pressure. Finally, Zn(II) is one of the crucial nutrients that does not produce in the body naturally. This ion contributes to skin health and growth with a critical role in immune function and DNA synthesis. Even though Zn(II) deficiency can harm the body, higher doses may exhibit consequents like headache, nausea and diarrhea (Chasapis et al., 2020; Tubek, 2007).

Ion chromatography (Wang et al., 2020), atomic absorption spectroscopy (AAS) (Manjusha et al., 2019) and inductively-coupled-plasma mass spectrometry (ICP/MS) (Alexander et al., 2017) have been introduced as the common quantification techniques for these metals. Although the mentioned methods usually have shown higher sensitivity and selectivity, they are costly and their completion is hard. Moreover, intricate operations and processing time of the samples restrict throughout and several measurements (Piovesan et al., 2020; Abdulsahib et al., 2021; Aljeboree et al., 2020; Malakootian et al., 2021). However, electrochemistry has been considered as one of the candidate detection methods combined with affordable sensors for trace metal analysis. SWASV is usually employed to detect heavy metals because of its higher sensitivity which is one of the results of a preconcentration process, accumulating metal on the electrode surface (Pizarro et al., 2020; Aljeboree et al., 2021; Alshamusi et al., 2021).

Recently, experts in the field have dealt with the synthesis of diverse rare earth elements (Sm, Tb, Eu, Yb, Pr, Sr, Dy, Tm, & Gd) in the formula of oxides of metal, hexacyanoferrates of metal, and dopant metal that employed them for the modification of electrodes (Huang and Zhu, 2019; Ganduh et al., 2021). Amongst the above materials, the Tb ion owns a great ionic radius of 0.92 Å and several valence states (Tb^{4+} & Tb^{3+}), resulting in the orientation for generating higher electronic holes/charges and creation of the effective path of electron transfer. Hence, integrating the Tb^{3+} into the nano-materials lattice (e.g., metal oxides) largely enhances the electronic conductivity, sensing features as well as electrochemical performance (Wu et al., 2021; Ganduh et al., 2021). Now, the

perovskite-type ABO_3 nanoparticles (A = rare or alkali earth metals, BO_3 = transition metals oxides) have been employed by researchers in multiple areas like gas transducers, solar batteries, solid-electrolyte batteries, magnetic sensors, and catalysts (Ahmad et al., 2020; Jasim et al., 2022). Even though other investigations have shown numerous achievements in reducing resistance, poor conductivity and particle aggregation have seriously constrained the uses and performances of the perovskite-type oxides. The copper oxide (CuO) as a p-type semiconductor metal oxide with the narrow bandgap (nearly 1.3–2.2 eV) possess suitable properties for sensor development such as low price, abundance in nature, high specific surface area, good electrochemical activity, excellent stability and proper redox potentials. Hence, the incorporation of $TbFeO_3$ NPs and CuO, could display a hybrid nano-composite that ameliorates the rate of electron transfer and create a higher surface area of electrochemical sensors (Ibarlucea et al., 2020; Mahdi et al., 2021).

Recently, research has focused on the design of environmental-friendly processes and products because of the issues regarding the changes in climate, water pollution, human health, and limited natural resources. For this reason, some methods have been presented for improving the production of NPs with the use of green techniques (Khorasanizadeh et al., 2019). In this way, the synthesis of the $TbFeO_3/CuO$ composite was performed according to the green approaches. In this regard, Crataegus and *Lantana Camara* leave as fuel and alkalizing agents respectively were employed. Additionally, we utilized $TbFeO_3/CuO$ for modifying CPE and also employed SWASV for selective detecting of Pb(II), Zn(II) and Cd(II) (Scheme 1). In the end, $TbFeO_3/CuO/CPE$ was applied to the determination of these ions simultaneously in the milk, apple juice and water.

2. Experimental

2.1. Materials and methods

Each reagent used in this study was of analytic grade. We choose Merck Co. (Darmstadt, Germany) for obtaining Cu $(NO_3)_2 \cdot 3H_2O$, $Fe(NO_3)_3 \cdot 9H_2O$, $Tb(NO_3)_3 \cdot 6H_2O$ as well as standard solution of zinc (($Zn(NO_3)_2$, 1000 ppm), lead (($Pb (NO_3)_2$, 1000 ppm) and cadmium ($CdCl_2$, 1000 ppm). The ultra-pure water was used to provide the chemical solution.

In the next step, each electrochemical measurement was conducted with 797 computrace software and a Metrohm 797 apparatus. Moreover, a three-electrode cell including a platinum wire as a counter electrode, an Ag/AgCl (3 M KCl) as the reference electrode and a bare or modified CPE as the working electrode was employed. For the recording of NP XRD patterns, a diffractometer with Cu Ka radiation (k = 1.54 Å) was employed (Philips). In addition, the dimension and morphology of $TbFeO_3/$ CuO nanocomposite were studied using scanning electron microscope (TESCAN Mira3 XMU).
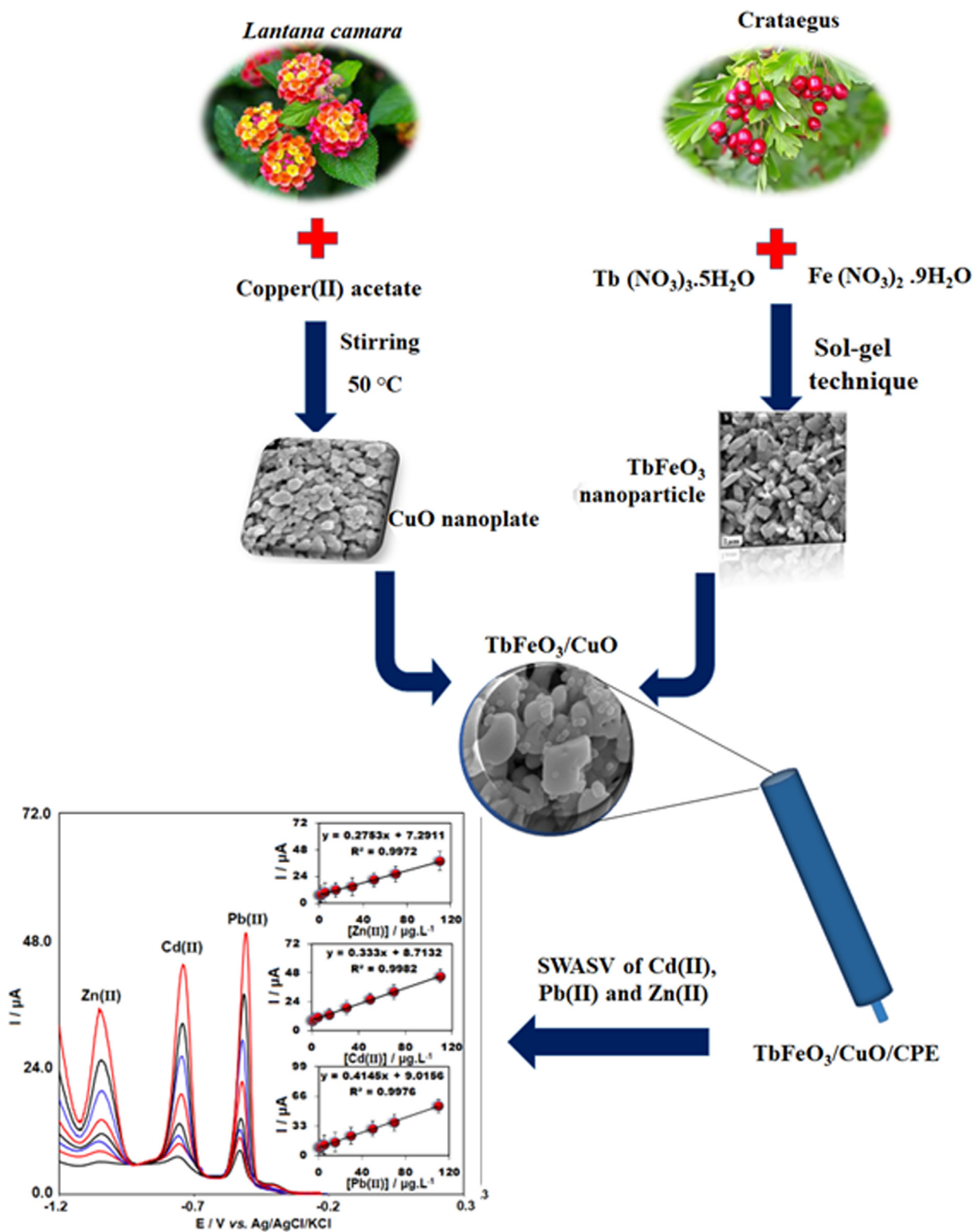
Scheme 1 Development of the modified sensor for simultaneous determination of Zn(II), Cd(II) and Pb(II).

2.2. Preparation of TbFeO₃ nanoparticles

In this section, we used a sol–gel technique for the synthesis of perovskite $TbFeO_3$ NPs. $Fe\ (NO_3)_2 \cdot 9H_2O$ and $Tb(NO_3)_3 \cdot$ $6H_2O$ with 1:1 stoichiometric ratio dissolved in ultrapure water (20 mL). In the following step, the extracted Crataegus (10 mL) was poured into the above solution at 80 °C and stirred for sixty minutes. By heating the solution to 180 °C, a gel-

like product was obtained and dried at 75 °C for a day. Finally, the calcination of the product was done at 800 °C for four hours.

2.3. Preparation of Lantana camara leaves extract

Lantana Camara leaves were collected from Ghaem Forest in Kerman, Iran. Fresh Leaves of Lantana Camara were washed 3 times and finally dried at 25 °C. Dried leaves were pulverized mechanically, sieved and poured into distilled water for three days. The final solution was concentrated at 40 °C and reduced pressure using a rotary flash evaporator. Next, the drying of the product was done in an oven at 60 °C.

2.4. Preparation of CuO NPs

A precipitation procedure using extract of Lantana Camara leaves as the alkalizing agent and copper(II) acetate as a precursor was done for the synthesis of CuO NPs. The extracted plant (2.5 wt%), copper(II) acetate solution and 25 mL of water were mixed under stirring at 70 °C. Next, the mixture was cooled to ambient temperature. After the centrifugation of the mixture at 5000 rpm, the washing of the final product was performed with water and an oven with 60 °C was used for drying of NPs for 12 h. Lastly, the obtained NPs were calcinated in a furnace at 400 °C for two hours for purification.

2.5. Synthesis of TbFeO₃/CuO nanocomposite

A one-pot simple mixing-sonication technique for the preparation of $TbFeO_3/CuO$ nanocomposites was applied. In a typical procedure, a sample containing $TbFeO_3$ nanoparticles with the appropriate amount of CuO was grounded in an agate mortar for 5 min. Finally, sonication of the mixed powder in distilled water was done for 15 min and agitated for one day. The obtained product was dried in the oven at 60 °C for 24 h.

2.6. Modified electrode preparation

The $TbFeO_3/CuO/CPE$ was developed by blending $TbFeO_3/CuO$ nanocomposite (10% w/w) and graphite powder in the presence of 0.5 mL paraffin oil to get a homogeneous mixture for 20 min. The obtained paste was transferred to the glassy tube and a copper wire was utilized for the electrical contact.

2.7. Real sample preparation

Pasteurized milk, apple juice and drinking water samples were collected from the local market in Kerman (Iran). For the preparation of drinking water and apple juice samples, all suspended particles were eliminated by filtering the samples and analysis was performed via setting pH at 4.8 by acetate buffer solution (ABS). In addition, ultra-sonication-assisted acid digestion was employed for treating the milk samples. For this reason, 50 μL of H_2O_2 (30 wt%) was poured into the milk sample (20 mL) and sonication was performed for 15 min. After that, we poured 5 mL glacial acetic acid and 5 mL HCl into the solution and proceeded to sonication for 8 min. Afterward, the mixture was centrifuged at 7000 r.p.m. for 10 min. In the final step, we poured the filtered sample solution

into the container and adjusted the pH at 4.8 by 0.1 M sodium hydroxide solution and diluted it with the ultrapure water to 50 mL before moving it to the electrochemical cell.

2.8. Electrochemical measurement

SWASV voltammograms were recorded at the modified CPE in the presence of Pb(II), Zn(II) and Cd(II) in the potential ranges between –1.2 and –0.2 V. Furthermore, they were accumulated at the potential of –1.2 V for 180 s followed by 5 s equilibration time. These ions were measured with a positive scan of potential in the amplitude of 50 mV, a frequency of 25 Hz and a potential step of 4 mV.

3. Results and discussion

3.1. Characterization of TbFeO₃/CuO nanocomposite

The XRD pattern of the $TbFeO_3/CuO$ nanocomposite is shown in Fig. 1A. In the XRD pattern, no impurity was observed and crystalline nanostructure was formed for the new nanocomposite. The synthesized nanoparticles in the presence of Crataegus were consistent with the JCPDS card No. 01–080-1268 of a monoclinic phase of CuO (Sorbiun et al., 2018) and perovskite-type $TbFeO_3$ (JCPDS card No. 47–0068) showed the successful development of $TbFeO_3/CuO$ nanocomposites. The calculation of the crystal size of $TbFeO_3/CuO$ was done using the Deby-Scherrer equation and was 35.04 nm.

(Fig. 1 1B. displays the EDS spectrum of the $TbFeO_3/CuO$ nanocomposite and confirms the presence of Cu, O, Tb, and Fe elements. Moreover, the uniform distribution of terbium, iron, oxygen and copper on the surface of nanocomposite can be seen from the mapping (Fig. 1C).

The SEM was used for analyzing the morphology of the present nanocomposite, indicating the development of nano-sized particles with uniform and smooth morphology at the surface of the nanocomposite with 50 nm size (Fig. 2A & B). It is obvious that SEM creates an image by detecting reflected or knocked-off electrons, while TEM uses transmitted electrons (electrons that are passing through the sample) to create an image. TEM images provide internal details of small samples at near-atomic resolution. Furthermore, we sent the samples for the transmission electron microscopy (TEM) image of the perovskite nanocomposite sample that is presented in Fig. 2C. Fig. 2C displayed the formation of nanosized particles at the surface of nanocomposite with uniform morphology and without any agglomeration. The obtained data of TEM is consistent with SEM results as well. Fig. 2D indicates the particle size histogram curve according to SEM image.

3.2. Electrochemical features of the electrodes

In this step, the electrochemical behavior of bare CPE (a), CuO/CPE (b) and $TbFeO_3/CuO/CPE$ (c) in 5 mM $[Fe(CN)_6]^{3-/4-}$ redox probe were investigated. As displayed in Fig. 3A, a pair of redox peaks were seen at CuO/CPE (curve b) and bare CPE (curve a). According to the recorded voltammograms, the peak current of a redox couple on the CuO/CPE surface was remarkably enhanced and ΔE_p declined, which can be caused
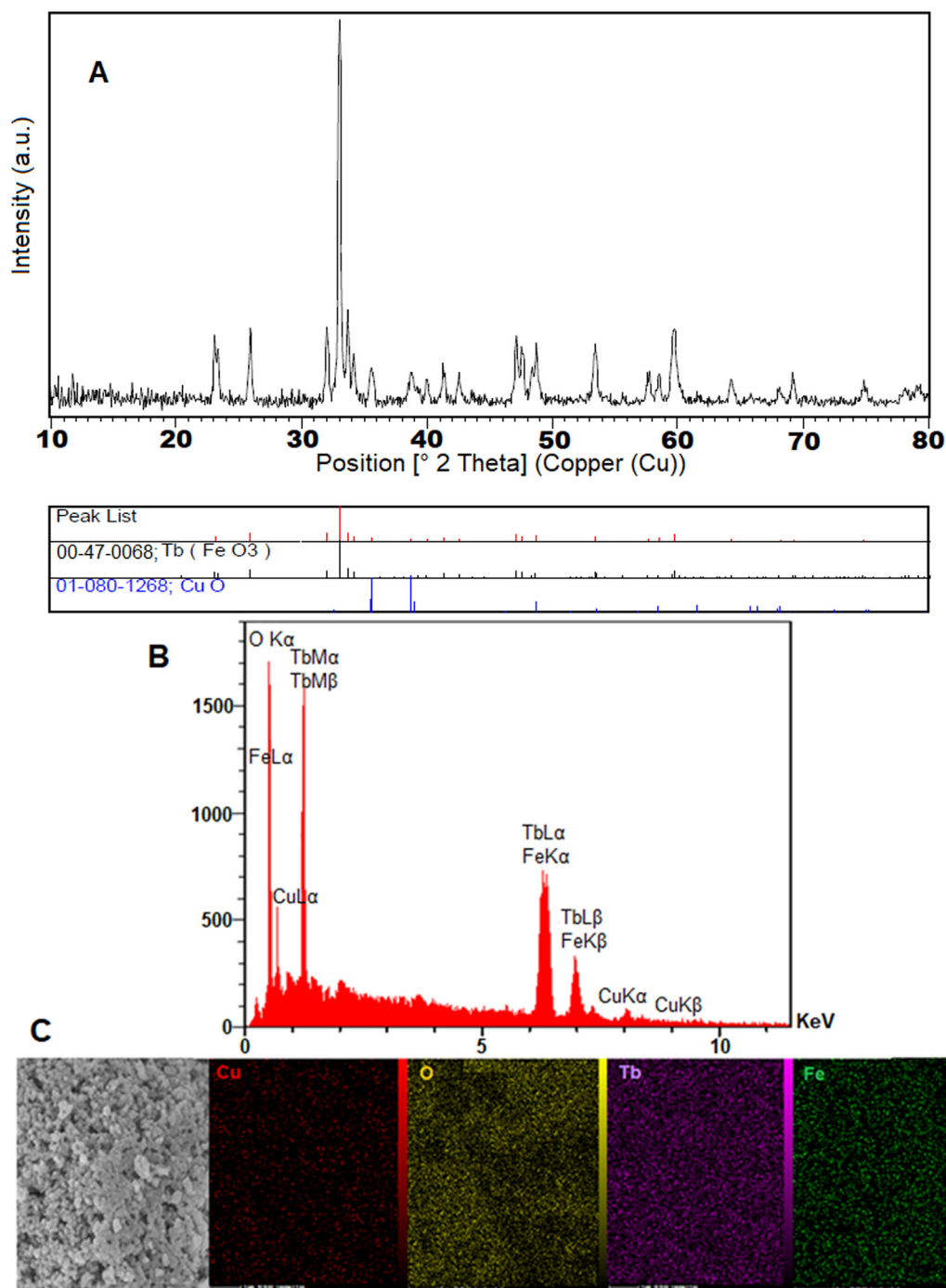
Fig. 1   A) XRD Pattern of TbFeO$_3$/CuO, B) EDS spectrum and C) map of TbFeO$_3$/CuO nanocomposite.

by the large surface area of the CuO NPs and acceleration of the electron transfer at the electrode surface, resulting in larger current signals. The comparison of redox response on the TbFeO$_3$/CuO/CPE (c) with CuO/CPE and bare CPE showed a higher redox peak current on TbFeO$_3$/CuO/CPE than on bare and CuO/CPE, probably due to the great surface area and synergistic impact of CuO and TbFeO$_3$ NPs, thereby improving the electrochemical behavior of the electrode. CuO is a component of catalysts with the extensive utilization to provide affordable sensors due to acceptable electrocatalytic

and electrochemical features, as well as good availability (Ahmad et al., 2017). Therefore, the integration of TbFeO$_3$ NPs and the p-type semi-conductor CuO with the nearly 1.2 eV bandgap, good stability and catalytic performance might present a hybrid nanocomposite with the synergistic features that enhance the rates of the electron transfer on the surface of the electrodes and exhibit reasonable bio-compatibility and higher surface areas.

In addition, CV was implemented for calculating the active surface area (A) of electrodes in the [Fe(CN)$_6$]$^{3-}$ solution at
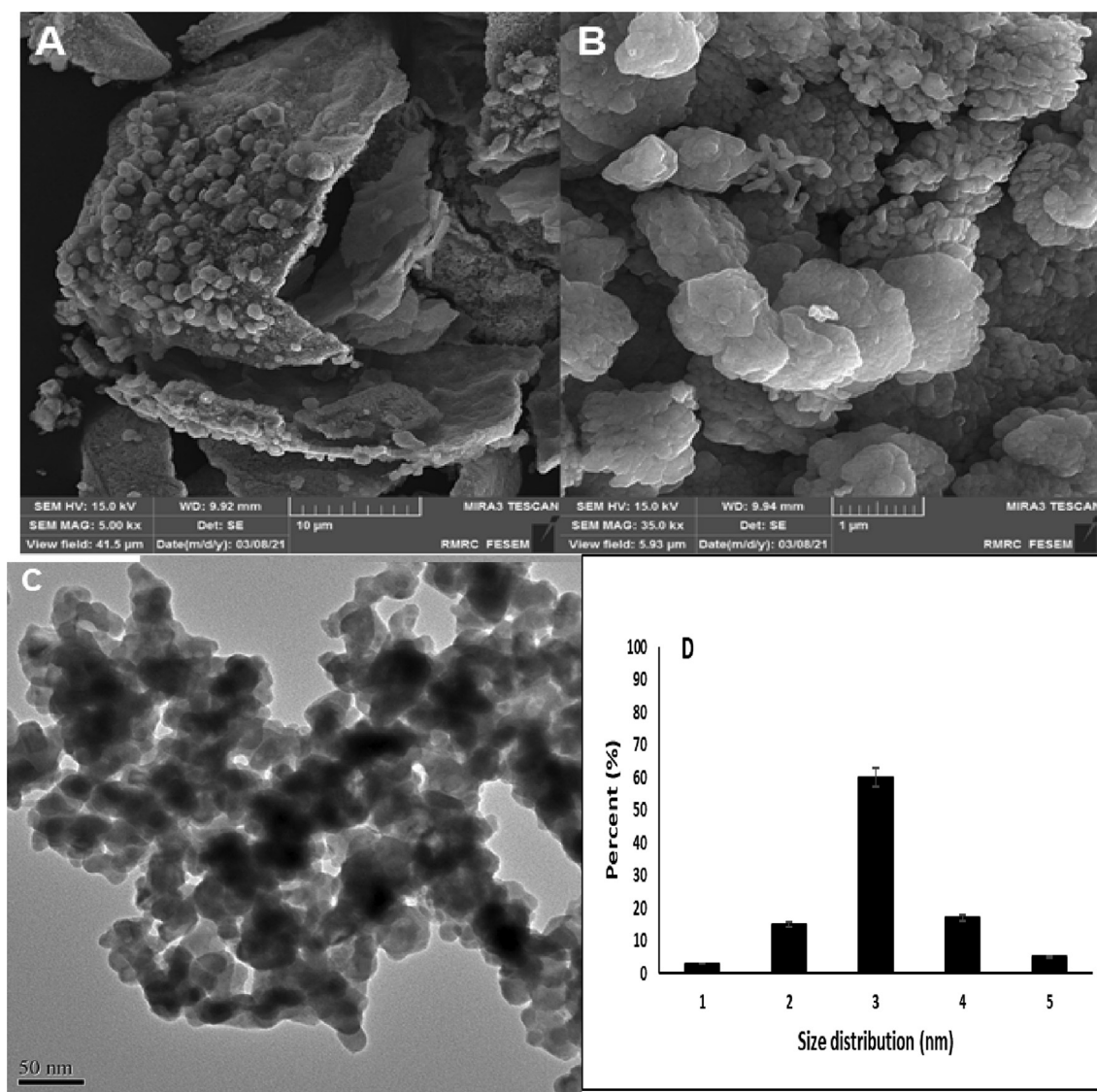
Fig. 2   A&B) SEM of TbFeO$_3$/CuO in two scales, C) TEM image of TbFeO$_3$/CuO and D) particle size histogram (1: samples under 30 nm, 2: 20–30 nm, 3:40–50 nm, 4: more than 50 nm).

diverse rates of the scan. Hence, Randles–Sevcik equation was applied for a reversible process of the electrode. The I_p has been defined by Eq. (1):

$$I_p = \pm(2.69 \times 10^5)n^{3/2}AD^{1/2}Cv^{1/2} \tag{1}$$

where n refers to the number of electrons engaged in the redox reaction, A represents the electrode surface area (cm^2), D stands for the diffusion coefficient, and C refers to the K$_3$[Fe(CN)$_6$] concentration. In the next step, I_p plot vs. $v^{1/2}$ was employed to calculate the electroactive areas for bare and modified sensors. The electrochemical active surface area for the bare, CuO/CPE and TbFeO$_3$/CuO/CPE were computed 0.042, 0.121 and 0.159 cm^2, respectively.

In Fig. 3B, SWASV responses of 70 µg/L Pb(II), Cd(II) and Zn(II) are observed at bare and TbFeO$_3$/CuO/CPE in 0.1 M ABS (pH of 4.8). The bare CPE displayed 3 weak current peaks at −1.0, −0.71 and −0.49 V relative to the zinc, cadmium and lead ions, respectively. The larger surface areas of the CuO and TbFeO$_3$ which provided several active sites for electrochemical reactions and acceptable conductivity of new nanocomposite enhanced the stripping signals of zinc, lead and cadmium ions at TbFeO$_3$/CuO/CPE compared to the obtained signal of bare CPE.

3.3. Investigation of chemical and electrochemical parameters

In this section, the impact of the modifier %, potential and time accumulation as well as pH on the stripping response of three ions were studied. In the analysis step of optimal modifier%, the highest striping current was achieved to be nearly 10% (w/w) of TbFeO$_3$/CuO as a modifier for the development of CPE (Fig. 4A). The number of the available active site would be declined to accumulate the analyte at the lower ratios of modifier in the constructed TbFeO$_3$/CuO/CPE, causing lower current responses of the analyte. On the other hand, forming higher active sites at the surface of the modified elec-
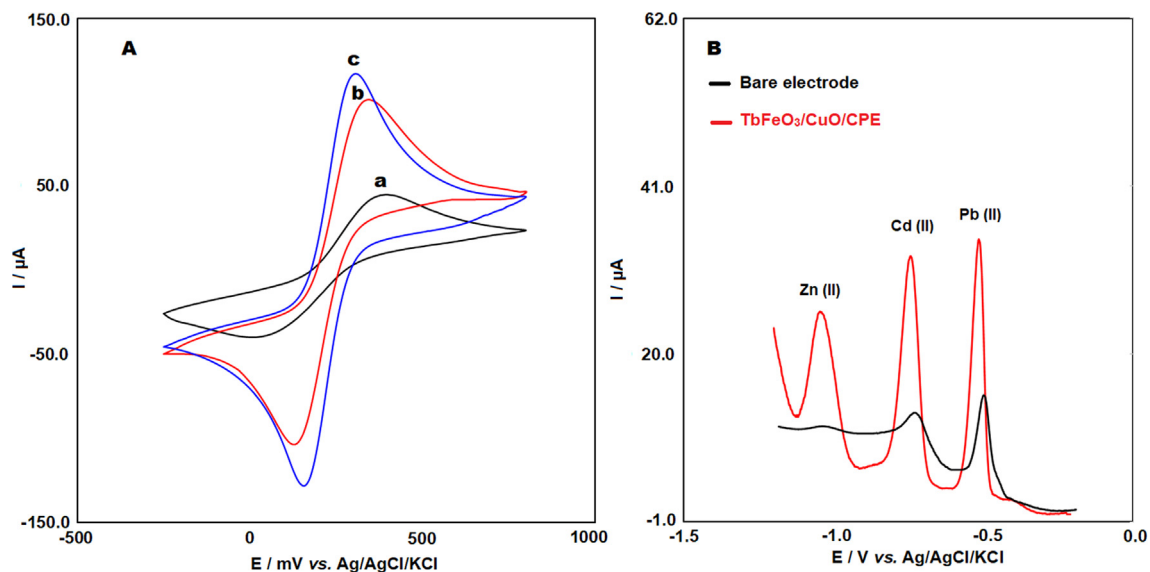
Fig. 3 A) Cyclic voltammograms of 5 mM $K_3[Fe(CN)_6]$ recorded on the bare CPE (a) CuO/CPE (b) and $TbFeO_3$/CuO/CPE (c), B) SWASV voltammograms of 70 µg/L Zn(II), Cd(II) and Pb(II) in the ABS (0.5 M, pH 4.8) on the bare CPE and $TbFeO_3$/CuO/CPE. Deposition potential: −1.2 V; Deposition time: 180 s.
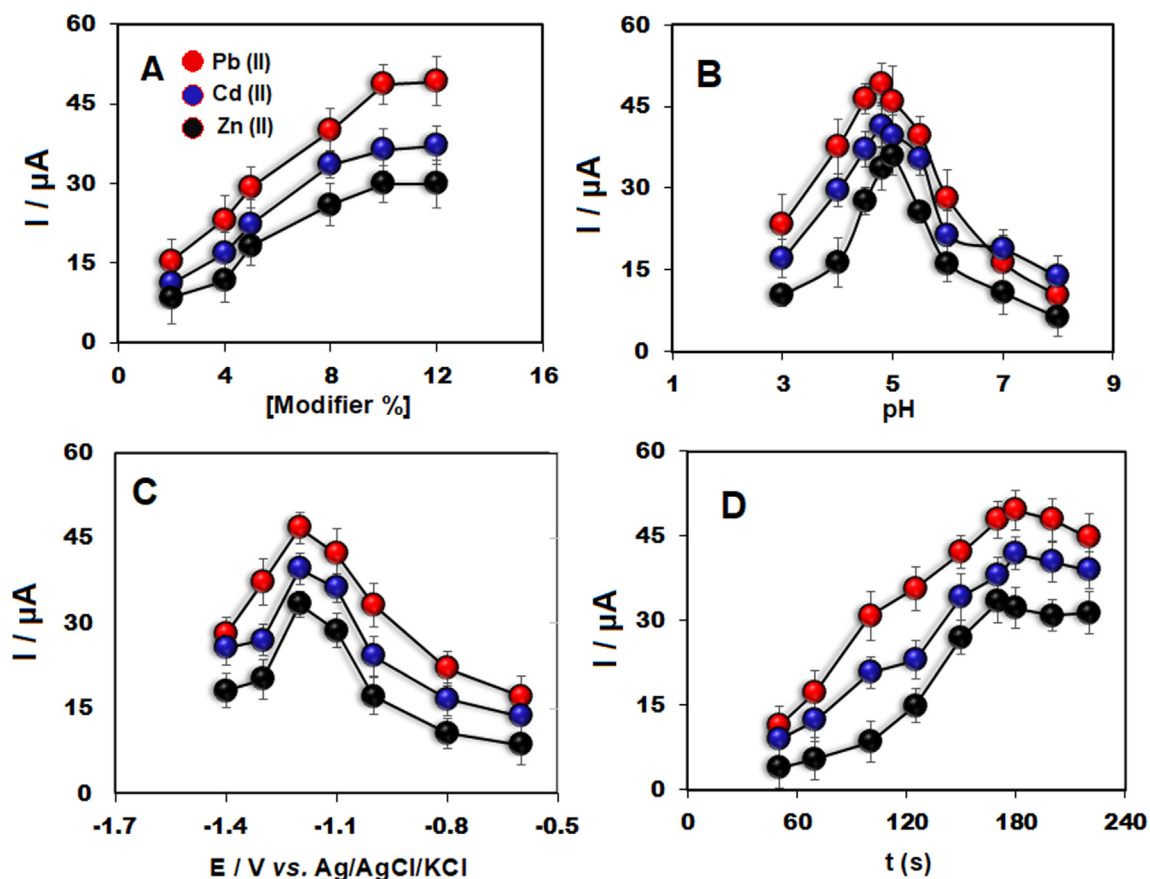
Fig. 4 Anodic peak currents for 110 µg/L Zn(II), Cd(II) and Pb(II) obtained by SWASV as the function of A) modifier%, B) pH, C) accumulation potential and D) accumulation time at the $TbFeO_3$/CuO/CPE (n = 3).

trode with the higher ratio of the modifier enabled the deposition of the electrode with an enhanced number of these ions.

Furthermore, the pH impact of the supporting electrolyte on the response of cadmium, lead and zinc ions was examined

in the range between 3.0 and 8.0. With regard to the outputs in Fig. 4B, the highest response at a pH of 4.8 was achieved. The lower current signals at a lower pH may be caused by electrostatic interactions and competition of the H^+ ions with metallic ions to be accrued on the negatively charged surface of electrodes. However, above the pH of 4.8, decreasing in the peak current could be related to the hydrolysis of these ions. Finally, the pH of 4.8 as the optimum value was selected.

The effects of accumulation potential (E_{acc}) on the signal of 110 µg/L Zn(II), Cd(II) and Pb(II) and were examined between −1.4 V and −0.6 V. Each measurement was repeated three times (n = 3) with an RSD of < 5%. As shown in Fig. 4C at the potentials < − 1.0 V the current signals were enhanced, reaching a maximum at −1.2 V for these ions. Moreover, decreasing the response of each ion at the potential more negative than −1.2 V was related to H_2 evolution. Hence, −1.2 V was selected as the optimal potential.

Fig. 4D depicts the dependence of the response of zinc, lead and cadmium with the time of accumulation (t_{acc}). As seen, the current signal of ions was enhanced by increasing t_{acc} until it reaches a maximum within 180 s. After that, any remarkable elevation was not seen, revealing the saturation of three ions at the modified electrode surface. Therefore, 180 s was used as the optimum deposition time for subsequent tests.

3.4. Determination of Pb(II), Zn(II) and Cd(II) using TbFeO₃/CuO/CPE

The stripping process of the mentioned ions for the verification of the practicality of TbFeO₃/CuO/CPE for simultaneous determination of Zn(II), Cd(II) and Pb(II) was done.

In this stage, the concentration of one ion changed, whereas the other ions remained constant. As demonstrated in Fig. 5A, the signal of zinc ion indicated a linear relation with its concentration between 0.9 and 110 µg/L in the case of a fixed concentration of lead and cadmium; however, Cd(II) and Pb(II) response did not alter with the enhanced concentration of Zn (II). Moreover, linear calibration graph for zinc showed
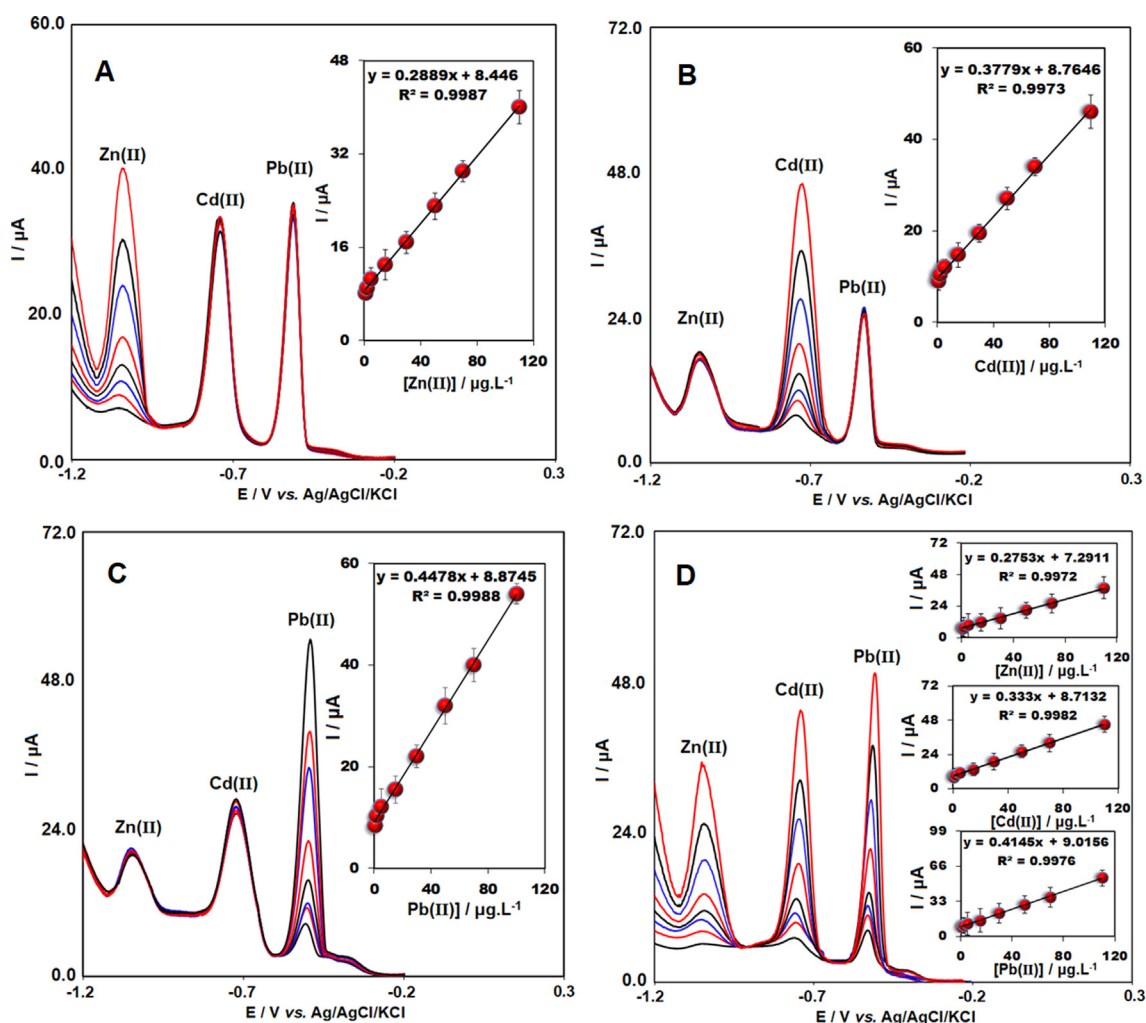
Fig. 5 Voltammograms of SWASV for determination of different concentrations of A) Zn(II), B) Cd(II) and C) Pb(II) (0.9–110 µg/L) in the presence of fixed concentration of other two ions at TbFeO₃/CuO/CPE. Insets: I_p vs. difference concentration of analytes. D) Voltammograms of SWASV for simultaneous determination of Zn(II), Cd(II) and Pb(II) at TbFeO₃/CuO/CPE in 0.5 M ABS (pH 4.8). From bottom to top, 0.9, 2.0, 5.0, 15.0, 30.0, 50.0, 70.0 and 110.0 µg/L for Zn(II), Cd(II) and Pb(II). Insets: the corresponding calibration curves of Zn(II), Cd(II) and Pb(II) (n = 3).

Table 1 Comparison of the present electrode with other electrochemical sensors for the Zn(II), Cd(II) and Pb(II) detection.

Modified electrode	Linear range Zn(II) (μg/L)	Linear range Cd(II) (μg/L)	Linear range Pb(II) (μg/L)	LOD of Zn (II) (μg/L)	LOD of Cd (II) (μg/L)	LOD of Pb (II) (μg/L)	Ref.
Bismuth/poly(p-aminobenzene sulfonic acid)	1–110	1–110	1–130	0.62	0.63	0.8	(Wu et al., 2008)
Clioquinol/HMDE	0–25	0–15	0–15	0.06	0.06	0.1	(Herrero et al., 2014)
Screen-printed carbon nanotubes electrodes	12–100	2–100	2–100	11	0.8	0.2	(Injang et al., 2010)
Nafion/G/PANI nanocomposite	1–300	1–300	1–300	1	0.1	0.1	(Ruecha et al., 2015)
AgNP/Bi/Nafion	5.0–400.0	5.0–400.0	0.1–500.0	5	0.5	0.1	(Mettakoonpitak et al., 2017)
GC/GQDs-NF	–	20–200	20–200	–	11.3	8.49	(Pizarro et al., 2020)
BiFE	5–110	5–110	5–110	1.07	0.93	0.65	(Thanh et al., 2019)
Hg-Bi/PDAAQ/GC	1–50	1–50	0.012–0.120	0.037	0.107	0.007	(Hassan et al., 2020)
Eu^{3+}–doped NiO/CPE	–	0.8–165	0.8–165	–	0.4	0.1	(Malakootian et al., 2020)
Bismuth film/N/IL/G/SPCE	1×10^{-4}–0.1	1×10^{-4}–0.1	1×10^{-4}–0.1	9×10^{-5}	6×10^{-5}	8×10^{-5}	(Chaiyo et al., 2016)
AgNPs@p-1,8-DAN/GC	–	$0.016–337.2$	$0.027–2.4 \times 10^{3}$	–	0.019	0.03	(Hassan et al., 2019)
BiNP/MWCNT-NNaM/PGE	$154.3–1.1 \times 10^{4}$	$35.9–2.7 \times 10^{4}$	$6.21-1.6 \times 10^{4}$	46.22	10.9	1.65	(Yıldız et al., 2022)
PEDOT/PVA/AgNPs/SPCE	10–80	10–80	10–80	6	3	8	(Ngoensawat et al., 2022)
Ala/GCE	0.65–653.8	0.84–843	–	0.58	0.64	–	(Kokab et al., 2019; Mahdi et al., 2020; Mahdi et al., 2022)
$TbFeO_3$/CuO/CPE	0.9–110	0.9–110	0.9–110	0.48	0.29	0.12	This study

$y = 0.2889x + 8.44$ ($R^2 = 0.998$). With regard to Fig. 5B & C, in the case of a fixed concentration of the other two metals, the signal of lead and cadmium experienced a linear increase with concentration. In addition, $y = 0.3779x + 8.7646$ ($R^2 = 0.998$) for linear regression equation of Cd(II) in the concentration range between 0.9 μg/L and 110 μg/L was obtained. Furthermore, linear regression equation for Pb(II) was $y = 0.4478x + 8.87$ ($R^2 = 0.998$) in the concentration range between 0.9 and 110 μg/L. Hence, clear separation of the stripping peak of the mentioned metals in the ternary mixture containing cadmium, lead and zinc was observed. Consequently, LOD was calculated 0.29 μg/L for cadmium, 0.12 μg/L for lead and 0.48 μg/L for zinc ions, respectively.

A comparison was made between the analytic function of the present sensor and other investigated sensors for cadmium, lead and zinc determination (Table 1). With regard to the results, $TbFeO_3$/CuO/CPE exhibited a broader dynamic range and smaller LOD than some of sensors. Furthermore, the low-cost and green materials employed in the fabrication of $TbFeO_3$/CuO/CPE resulted in its attractiveness for analyzing heavy metals.

The $TbFeO_3$/CuO/CPE was also employed for simultaneous detection of cadmium, lead and zinc ions. Fig. 5D shows the SWASV voltammogram of three ions mixture in a range from 0.9 to 110 μg/L. As shown, three distinct and completely resolved peaks were obtained at nearly -1.0, -0.73 V and $- 0.51$ for zinc, cadmium and lead, respectively. Furthermore, linear range and sensitivity remained constant and no shifts close to the peak position of Zn(II), Cd(II) and Pb(II) in comparison to their independent detection were not observed, demonstrating the minimum mutual interferences between cadmium, lead and zinc ions. Therefore, due to the entire separation of the above three peaks, simultaneous determination of these ions using $TbFeO_3$/CuO/CPE is possible.

3.5. Stability, reproducibility and repeatability

The SWASV was employed to study the reproducibility, stability and repeatability of the modified electrode in the presence of 50 μg/L of three ions. Five independent $TbFeO_3$/CuO/CPEs were analyzed for investigating the ability for the reproduction of the modified electrode and relative standard deviations (RSD%) 3.32, 3.14 and 3.44 achieved for zinc, cadmium and lead ions, respectively. Moreover, 10 replicate measurements of 50 μg/L Cd(II), Zn(II) and Pb(II) were performed and RSD% for peak currents were 2.41, 2.62 and 2.18, respectively. Then, the stability of the modified electrode for four weeks via repetition of measurement once a week was performed. According to the analysis, the new electrode displayed long-term stability and kept $\sim 94.9\%$ of the initial current which would be favorable for analytical applications.

3.6. Investigating the effects of interferences

We accomplished interference experiments with the addition of diverse ions into a solution consisting of 10 μg/L of three ions in 0.1 M ABS (pH of 4.8) (Fig. 6). Based on $\pm 5.0\%$ tolerated ratio, the 250-fold concentration of K(I), Mg(II), Ca(II) and Na(I); 100-fold concentration of Fe(II), Al(III), Hg(II) and 25-fold concentration of Cu^{2+} showed no interfering in analyzing of three ions. The inhibitory impact of Cu^{2+} can be
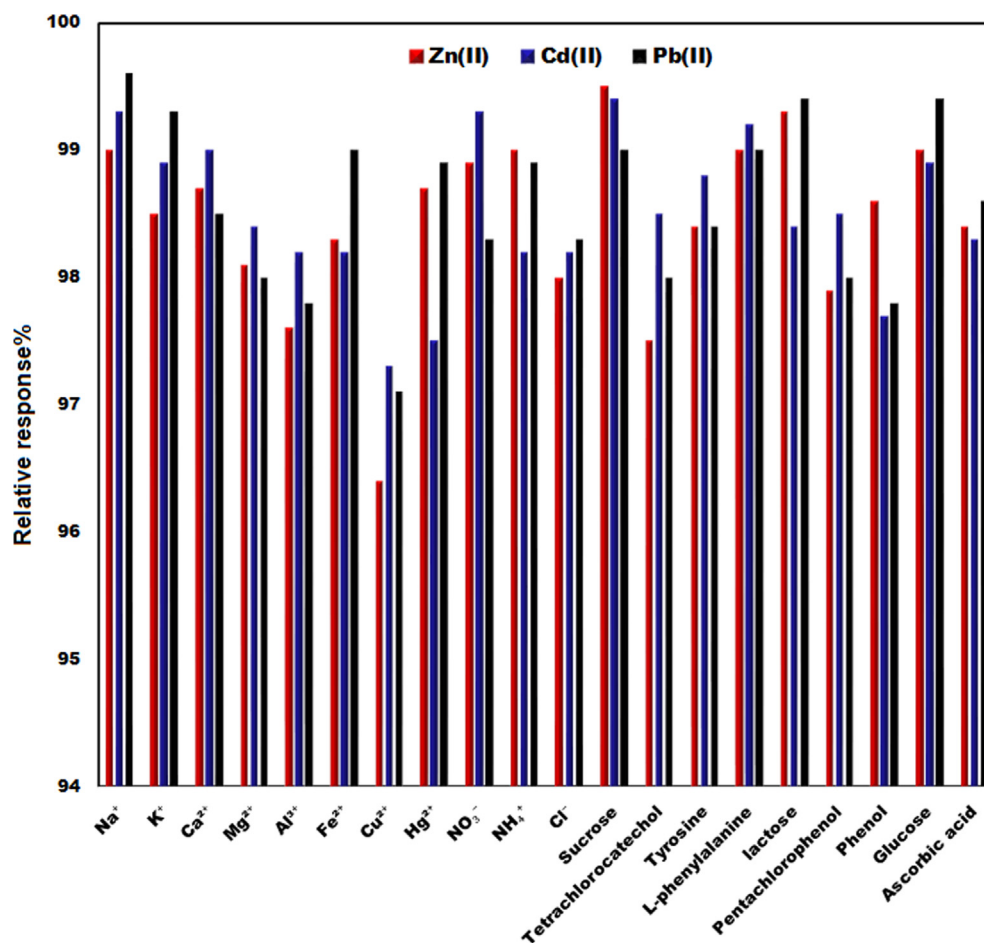
Fig. 6 The relative signals of TbFeO$_3$/CuO/CPE in the presence of 10.0 µg/L of Zn(II), Cd(II) and Pb(II) and other interfering compounds.

Table 2 Determination of Zn(II), Cd(II) and Pb(II) in real samples using TbFeO$_3$/CuO/CPE (n = 3).

Sample	Zn(II) Spiked (µg/L)	Zn(II) Found (µg/L)	Recovery (%) Zn(II	RSD (%)	Cd(II) Spiked (µg/L)	Cd(II) Found (µg/)	Recovery (%) Cd (II)	RSD (%)	Pb(II) Spiked (µg/L)	Pb(II) Found (µg/L)	Recovery (%) Pb (II)	RSD (%)
Drinking water	0.0	13.5	–	2.9	0.0	0.09	–	3.2	0.0	0.1	–	2.9
	3.0	16.0	97.0	2.6	10.0	10.4	103.0	2.8	5.0	4.9	96.0	3.1
	9.0	22.0	97.7	2.0	20.0	19.5	97.0	2.5	10.0	9.9	98.0	2.6
	12.0	26.2	102.7	2.1	30.0	29.7	98.7	2.0	15.0	15.5	102.6	2.2
Apple juice	0.0	26.2	–	2.6	0.0	0.9	–	3.1	0.0	0.5	–	3.2
	5.0	31.8	102.0	2.5	3.0	3.8	97.4	3.2	10.0	10.3	98.0	2.2
	10.0	35.5	98.0	1.9	9.0	10.3	104.0	2.4	20.0	21.0	102.4	2.5
	15.0	42.2	102.4	2.3	12.0	12.5	96.8	2.6	30.0	31.2	102.3	2.0
Pasteurized milk	0.0	98.3	–	2.2	0.0	0.2	–	3.3	0.0	N.D	–	–
	10.0	107.0	98.8	1.8	5.0	5.3	102.0	2.7	5.0	5.1	102.0	2.8
	20.0	120.1	101.5	2.3	10.0	10.6	103.9	2.4	10.0	9.8	98.0	2.4
	30.0	130.6	102.0	2.0	15.0	14.8	97.3	2.6	15.0	20.7	103.0	2.9

due to the competition of copper with the target metal ions for active sites at the TbFeO$_3$/CuO/CPE. Based on the masking effect of potassium ferrocyanide for Cu(II), we applied 0.5 µM potassium ferrocyanide for the copper elimination in detecting zinc, lead and cadmium ions.

Additionally, some organic materials such as phenol, glucose, ascorbic acid, sucrose, pentachlorophenol, tetrachlorocatechol, L-phenylalanine, tyrosine and lactose as probable interfering materials were examined in the presence of Pb(II), Zn(II) and Cd(II). According to the outcomes, adding the

Table 3 Comparing the analytical data for Zn(II), Cd(II) and Pb(II) detection in real samples with SWASV and ICP/MS (n = 3).

Sample	Zn(II) Spiked (µg/L)	Zn(II) Found (µg/L)		t	Cd(II) Spiked (µg/L)	Cd(II) Found (µg/L)		t	Pb(II) Spiked (µg/L)	Pb(II) Found (µg/L)		t
		SWASV	ICP/MS			SWASV	ICP/MS			SWASV	ICP/MS	
Drinking water	0.0	13.5 ± 0.4	13.1 ± 0.3	1.38	0.0	0.09 ± 0.003	0.15 ± 0.3	0.35	0.0	0.1 ± 0.003	0.2 ± 0.2	0.86
	3.0	16.0 ± 0.4	16.6 ± 0.5	1.62	10.0	10.4 ± 0.3	10.8 ± 0.5	1.19	5.0	4.9 ± 0.2	4.6 ± 0.4	1.16
	9.0	22.0 ± 0.5	22.7 ± 0.3	2.07	20.0	19.5 ± 0.5	20.2 ± 0.7	1.4	10.0	9.9 ± 0.3	10.4 ± 0.4	1.73
Apple juice	0.0	26.2 ± 0.7	25.8 ± 0.4	0.86	0.0	0.9 ± 0.03	1.2 ± 0.6	0.86	0.0	0.5 ± 0.02	0.8 ± 0.5	1.04
	5.0	31.8 ± 0.8	31.2 ± 0.6	1.04	3.0	3.8 ± 0.1	3.6 ± 0.4	0.84	10.0	10.3 ± 0.2	11.0 ± 0.7	1.66
	10.0	35.5 ± 0.7	35.0 ± 0.5	1.01	9.0	10.3 ± 0.2	10.9 ± 0.5	1.93	20.0	21.0 ± 0.5	20.9 ± 0.4	0.27

mentioned substances up to 100-fold did not impact the signal of the $TbFeO_3/CuO/CPE$ for zinc, cadmium and lead ions, which implies the reasonable selectivity of this approach and its functions for quantifying three ions in the real samples.

3.7. Cd(II), Zn(II) and Pb(II) determination in real samples

For studying the reliability of practical applications, $TbFeO_3/CuO/CPE$ was utilized to determine lead, zinc and cadmium ions in the real samples. Table 2 reports experimental outputs. For all ions, the recovery was < 104 % and greater than 97 %, revealing the potential of this modified electrode for the determination of these ions. Moreover, acceptable RSDs and recoveries and implied the reproducibility and precision of the modified electrode. In addition, the determination of ions was done by ICP-MS and the modified electrode in real samples and for comparison of the results the paired t-test was used (Table 3). Due to smaller t-values than the critical t-value, the null hypothesis would be confirmed. Hence, the new method with 95% confidence did not display different results.

4. Conclusion

In this study, we addressed the optimization of one of the highly affordable and environmental-friendly electrodes to detect Pb(II), Zn(II) and Cd(II) in the milk and drink samples simultaneously. According to the analyses, $TbFeO_3/CuO/CPE$ showed more electrocatalytic behavior for the determination of ions than the bare sensor. Moreover, a linear range between 0.9 and 110 µg/L with a LOD equal to 0.29, 0.12 and 0.48 µg/L for cadmium, lead, and zinc was calculated at optimum conditions. Finally, it was found that the $TbFeO_3/CuO/CPEs$ possess great potential for the detection of zinc, lead and cadmium in the water and food samples.

CRediT authorship contribution statement

Hadi Mahmoudi-Moghaddam: Project administration, Validation, Data curation, Formal analysis, Methodology, Investigation, Software. **Mahnaz Amiri:** Data curation, Investigation, Software, Methodology, Writing – original draft, Project administration. **Hamid Akbari Javar:** Data curation, Investigation, Software. **Qahtan A. Yousif:** Data curation, Investigation, Writing – review & editing, Software. **Masoud Salavati-Niasari:** Formal analysis, Methodology, Writing – review & editing, Writing – original draft, Conceptualization, Supervision, Project administration, Investigation, Data curation, Validation, Resources, Visualization, Funding acquisition.

Declaration of Competing Interest

The authors declare that they have no known competing financial interests or personal relationships that could have appeared to influence the work reported in this paper.

Acknowledgement

References

Paithankar, J.G., Saini, S., Dwivedi, S., Sharma, A., Chowdhuri, D. K., 2021. Heavy metal associated health hazards: an interplay of oxidative stress and signal transduction. Chemosphere 262,. https://doi.org/10.1016/j.chemosphere.2020.128350 128350.

Azeh Engwa, G., Udoka Ferdinand, P., Nweke Nwalo, F., Unachukwu, M.N., 2019. Mechanism and Health Effects of Heavy Metal Toxicity in Humans. Poisoning Mod. World - New Tricks Old Dog? 10 https://doi.org/10.5772/intechopen.82511.

Vardhan, K.H., Kumar, P.S., Panda, R.C., 2019. A review on heavy metal pollution, toxicity and remedial measures: current trends and future perspectives. J. Mol. Liq. 290,. https://doi.org/10.1016/j.molliq.2019.111197 111197.

Huang, Y.-H., Hsueh, C.-L., Huang, C.-P., Su, L.-C., Chen, C.-Y., 2007. Adsorption thermodynamic and kinetic studies of Pb(II) removal from water onto a versatile Al2O3-supported iron oxide. Sep. Purif. Technol. 55, 23–29.

Chasapis, C.T., Ntoupa, P.-S.-A., Spiliopoulou, C.A., Stefanidou, M. E., 2020. Recent aspects of the effects of zinc on human health. Arch. Toxicol. 94, 1443–1460.

Tubek, S., 2007. Zinc supplementation or regulation of its homeostasis: advantages and threats. Biol. Trace Elem. Res. 119, 1–9.

Wang, Y., Lou, S., Liu, X., Zhang, L., 2020. Detection of trace metal ions in high-purity boric acid by online two-dimensional valve switching coupled with ion chromatography-inductively coupled plasma mass spectrometry. Microchem. J. 155,. https://doi.org/10.1016/j.microc.2020.104661 104661.

Manjusha, R., Shekhar, R., Kumar, S.J., 2019. Ultrasound-assisted extraction of Pb, Cd, Cr, Mn, Fe, Cu, Zn from edible oils with tetramethylammonium hydroxide and EDTA followed by determination using graphite furnace atomic absorption spectrometer. Food Chem. 294, 384–389. https://doi.org/10.1016/j.foodchem.2019.04.104.

Alexander, D., Ellerby, R., Hernandez, A., Wu, F., Amarasiriwardena, D., 2017. Investigation of simultaneous adsorption properties of Cd, Cu, Pb and Zn by pristine rice husks using ICP-AES and LA-ICP-MS analysis. Microchem. J. 135, 129–139. https://doi.org/10.1016/j.microc.2017.08.001.

Piovesan, J.V., Santana, E.R., Spinelli, A., 2020. A carbon paste electrode improved with poly(ethylene glycol) for tannic acid surveillance in beer samples. Food Chem. 326,. https://doi.org/10.1016/j.foodchem.2020.127055 127055.

Abdulsahib, W.K., Sahib, H.H., Mahdi, M.A., Jasim, L.S., 2021. Adsorption Study of cephalexin monohydrate drug in solution on poly (vinyl pyrrolidone-acryl amide) hydrogel surface. Int. J. Drug Deliv. Technol. 11 (4), 1169–1172. https://doi.org/10.25258/ijddt.11.4.9.

Aljeboree, A.M., Alrazzak, N.A., Alqaraguly, M.B., Mahdi, M.A., Jasim, L.S., Alkaim, A.F., 2020. Adsorption of pollutants by using low-cost (Environment-Friendly): equilibrium, kinetics and thermodynamic studies: a review. Syst. Rev. Pharm. 11 (12), 1988–1997. https://doi.org/10.31838/srp.2020.12.303.

Malakootian, M., Hamzeh, S., Mahmoudi-Moghaddam, H., 2021. A novel electrochemical sensor based on FeNi3/CuS/ BiOCl modified carbon paste electrode for determination of bisphenol A. Electroanalysis 33, 38–45. https://doi.org/10.1002/elan.202060205.

Pizarro, J., Segura, R., Tapia, D., Navarro, F., Fuenzalida, F., Jesús Aguirre, M., 2020. Inexpensive and green electrochemical sensor for the determination of Cd(II) and Pb(II) by square wave anodic stripping voltammetry in bivalve mollusks. Food Chem. 321,. https://doi.org/10.1016/j.foodchem.2020.126682 126682.

Aljeboree, A.M., Mohammed, R.A., Mahdi, M.A., Jasim, L.S., Alkaim, A.F., 2021. Synthesis, characterization of p(Ch/aa-co-am) and adsorptive removal of pb (ii) ions from aqueous solution: thermodynamic study. NeuroQuantology 19 (7), 137–143. https://doi.org/10.14704/nq.2021.19.7.NQ21096.

Alshamusi, Q.K.M., Alzayd, A.A.M., Mahdi, M.A., Jasim, L.S., Aljeboree, A.M., 2021. Adsorption of crystal violate (CV) dye in aqueous solutions by using P(PVP-CO-AAM)/GO composite as (eco-healthy adsorbate surface): characterization and thermodynamics studies. Biochem. Cell. Arch. 21, 2423–2431.

Huang, H., Zhu, J.J., 2019. The electrochemical applications of rare earth-based nanomaterials. Analyst 144, 6789–6811. https://doi.org/10.1039/c9an01562k.

Ganduh, S.H., Aljeboree, A.M., Mahdi, M.A., Jasim, L.S., 2021. Spectrophotometric determination of metoclopramide-HCL in the standard raw and it compared with pharmaceuticals. J. Pharma. Neg. Res. 12 (2), 44–48. https://doi.org/10.47750/pnr.2021.12.02.008.

Wu, K.Y., Chen, M., Huang, N.H., Li, R.T., Pan, W.L., Zhang, W.H., Chen, W.H., Chen, J.X., 2021. Facile and recyclable dopamine sensing by a label-free terbium(III) metal−organic framework. Talanta 221,. https://doi.org/10.1016/j.talanta.2020.121399 121399.

Ganduh, S.H., Kmal, R.Q., Mahdi, M.A., Aljeboree, A.M., Jasim, L. S., 2021. Selective spectrophotometric determination of 4-amino antipyrine antibiotics in pure forms and their pharmaceutical formulations. Int. J. Drug Deliv. Technol. 11 (2), 371–375. https://doi.org/10.25258/ijddt.11.2.23.

Ahmad, K., Kumar, P., Mobin, S.M., 2020. Hydrothermally grown novel pyramids of the CaTiO 3 perovskite as an efficient electrode modifier for sensing applications. Mater. Adv. 1, 2003–2009. https://doi.org/10.1039/d0ma00303d.

Jasim, L. S., Aljeboree, A. M., Sahib, I. J., Mahdi, M. A., Abdulrazzak, F. H., & Alkaim, A. F. (2022). *Effective adsorptive removal of riboflavin (RF) over activated carbon.* AIP Conference Proceedings **2386**, 030030 (2022); https://doi.org/10.1063/5.0066996.

Ibarlucea, B., Pérez Roig, A., Belyaev, D., Baraban, L., Cuniberti, G., 2020. Electrochemical detection of ascorbic acid in artificial sweat using a flexible alginate/CuO-modified electrode. Microchim. Acta 187, 1–11. https://doi.org/10.1007/s00604-020-04510-5.

Mahdi, M.A., Aljeboree, A.M., Jasim, L.S., Alkaim, A.F., 2021. Synthesis, characterization and adsorption studies of. a graphene oxide/polyacrylic acid nanocomposite hydrogel. NeuroQuantology 19 (9), 46–54. https://doi.org/10.14704/nq.2021.19.9.NQ21136.

Khorasanizadeh, M.H., Monsef, R., Amiri, O., Amiri, M., Salavati-Niasari, M., 2019. Sonochemical-assisted route for synthesis of spherical shaped holmium vanadate nanocatalyst for polluted waste water treatment. Ultrasonics Sonochem. 58, 104686–104697.

Sorbiun, M., Shayegan Mehr, E., Ramazani, A., Taghavi Fardood, S., 2018. Green synthesis of zinc oxide and copper oxide nanoparticles using aqueous extract of oak fruit hull (Jaft) and comparing their photocatalytic degradation of basic violet 3. Int. J. Environ. Res. 12, 29–37. https://doi.org/10.1007/s41742-018-0064-4.

Ahmad, R., Tripathy, N., Ahn, M.-S., Bhat, K.S., Mahmoudi, T., Wang, Y., Yoo, J.-Y., Kwon, D.-W., Yang, H.-Y., Hahn, Y.-B., 2017. Highly efficient non-enzymatic glucose sensor based on CuO modified vertically-grown ZnO nanorods on electrode. Sci. Rep. 7, 5715. https://doi.org/10.1038/s41598-017-06064-8.

Wu, Y., Li, N.B., Luo, H.Q., 2008. Simultaneous measurement of Pb, Cd and Zn using differential pulse anodic stripping voltammetry at a bismuth/poly(p-aminobenzene sulfonic acid) film electrode. Sensors Actuators, B Chem. 133, 677–681. https://doi.org/10.1016/j.snb.2008.04.001.

Herrero, E., Arancibia, V., Rojas-Romo, C., 2014. Simultaneous determination of Pb2 + , Cd2 + and Zn 2 + by adsorptive stripping voltammetry using Clioquinol as a chelating-adsorbent agent. J. Electroanal. Chem. 729, 9–14. https://doi.org/10.1016/j.jelechem.2014.06.039.

Injang, U., Noyrod, P., Siangproh, W., Dungchai, W., Motomizu, S., Chailapakul, O., 2010. Determination of trace heavy metals in herbs by sequential injection analysis-anodic stripping voltammetry using screen-printed carbon nanotubes electrodes. Anal. Chim. Acta 668, 54–60. https://doi.org/10.1016/j.aca.2010.01.018.

Ruecha, N., Rodthongkum, N., Cate, D.M., Volckens, J., Chailapakul, O., Henry, C.S., 2015. Sensitive electrochemical sensor using a graphene-polyaniline nanocomposite for simultaneous detection of Zn(II), Cd(II), and Pb(II). Anal. Chim. Acta 874, 40–48. https://doi.org/10.1016/j.aca.2015.02.064.

Mettakoonpitak, J., Mehaffy, J., Volckens, J., Henry, C.S., 2017. AgNP/Bi/Nafion-modified disposable electrodes for sensitive Zn (II), Cd(II), and Pb(II) detection in aerosol samples. Electroanalysis 29, 880–889. https://doi.org/10.1002/elan.201600591.

Thanh, N.M., Van Hop, N., Luyen, N.D., Phong, N.H., Toan, T.T.T., Mai, H.D., 2019. Simultaneous determination of Zn(II), Cd(II), Pb (II), and Cu(II) using differential pulse anodic stripping voltammetry at a bismuth film-modified electrode. Adv. Mater. Sci. Eng. 2019, 1826148. https://doi.org/10.1155/2019/1826148.

Hassan, K.M., Gaber, S.E., Altahan, M.F., Azzem, M.A., 2020. Single and simultaneous voltammetric sensing of lead(II), cadmium(II) and zinc(II) using a bimetallic Hg-Bi supported on poly(1,2-diaminoanthraquinone)/glassy carbon modified electrode. Sens. Bio-Sensing Res. 29,. https://doi.org/10.1016/j.sbsr.2020.100369 100369.

Malakootian, M., Abolghasemi, H., Mahmoudi-Moghaddam, H., 2020. A novel electrochemical sensor based on the modified carbon paste using Eu3 + − doped NiO for simultaneous determination of Pb (II) and Cd (II) in food samples. J. Electroanal. Chem. 876,. https://doi.org/10.1016/j.jelechem.2020.114474 114474.

Chaiyo, S., Mehmeti, E., Žagar, K., Siangproh, W., Chailapakul, O., Kalcher, K., 2016. Electrochemical sensors for the simultaneous determination of zinc, cadmium and lead using a Nafion/ionic liquid/graphene composite modified screen-printed carbon electrode. Anal. Chim. Acta 918, 26–34. https://doi.org/10.1016/j.aca.2016.03.026.

Hassan, K.M., Elhaddad, G.M., AbdelAzzem, M., 2019. Voltammetric determination of cadmium(II), lead(II) and copper(II) with a glassy carbon electrode modified with silver nanoparticles deposited on poly(1,8-diaminonaphthalene). Microchim. Acta 186, 440. https://doi.org/10.1007/s00604-019-3552-0.

Yıldız, C., Eskiköy Bayraktepe, D., Yazan, Z., Önal, M., 2022. Bismuth nanoparticles decorated on Na-montmorillonite-multiwall carbon nanotube for simultaneous determination of heavy metal ions- electrochemical methods. J. Electroanal. Chem. 910,. https://doi.org/10.1016/j.jelechem.2022.116205 116205.

Ngoensawat, U., Pisuchpen, T., Sritana-anant, Y., Rodthongkum, N., Hoven, V.P., 2022. Conductive electrospun composite fibers based on solid-state polymerized Poly(3,4-ethylenedioxythiophene) for simultaneous electrochemical detection of metal ions. Talanta 241,. https://doi.org/10.1016/j.talanta.2022.123253 123253.

Kokab, T., Shah, A., Iftikhar, F.J., Nisar, J., Akhter, M.S., Khan, S. B., 2019. Amino acid-fabricated glassy carbon electrode for efficient simultaneous sensing of Zinc(II), Cadmium(II), Copper (II), and Mercury(II) ions. ACS Omega 4, 22057–22068. https://doi.org/10.1021/acsomega.9b03189.

Mahdi, M.A., Jasim, L.S., Mohamed, M.H., 2020. Synthesis and anticancer activity evaluation of novel ligand 2- [2 - (5-Chloro carboxy phenyl) Azo] 1-methyl imidazole (1-Mecpai) with some metal complexes. Syst. Rev. Pharm. 11 (12), 1979–1987. https://doi.org/10.31838/srp.2020.12.302.

Mahdi, M.A., Jasim, L.S., Ranjeh, M., Masjedi-Arani, M., Salavati-Niasari, M., 2022. Improved pechini sol-gel fabrication of Li2B4O7/NiO/Ni3(BO3)2 nanocomposites to advanced photocatalytic performance. Arabian J. Chem. 15 (5). https://doi.org/10.1016/j.arabjc.2022.103768.